Brain Stimulation 16 (2023) 879–888

Contents lists available at ScienceDirect

Brain Stimulation

journal homepage: www.journals.elsevier.com/brain-stimulation

Whole-brain network transitions within the framework of ignition and transfer entropy following VIM-MRgFUS in essential tremor patients

Julia M. Lueckel [a,1], Neeraj Upadhyay [a,1], Veronika Purrer [b,c], Angelika Maurer [a], Valeri Borger [d], Alexander Radbruch [e,b], Ulrike Attenberger [f], Ullrich Wuellner [b,c], Rajanikant Panda [g,2], Henning Boecker [a,b,2,*]

[a] Clinical Functional Imaging Group, Department of Diagnostic and Interventional Radiology, University Hospital Bonn, Bonn, Germany
[b] German Center for Neurodegenerative Diseases, Bonn, Germany
[c] Department of Neurology, University Hospital Bonn, Bonn, Germany
[d] Department of Neurosurgery, University Hospital Bonn, Bonn, Germany
[e] Department of Neuroradiology, University Hospital Bonn, Bonn, Germany
[f] Department of Diagnostic and Interventional Radiology, University Hospital Bonn, Bonn, Germany
[g] Coma Science Group, GIGA-Consciousness, University of Liège, Liège, Belgium

ARTICLE INFO

Keywords:
Essential tremor
MR-Guided focused ultrasound
Ventral intermediate nucleus
Information theory
Intrinsic ignition framework
Transfer entropy

ABSTRACT

Magnetic resonance-guided focused ultrasound (MRgFUS) lesioning of the ventralis intermedius nucleus (VIM) has shown promise in treating drug-refractory essential tremor (ET). It remains unknown whether focal VIM lesions by MRgFUS have broader restorative effects on information flow within the whole-brain network of ET patients. We applied an information-theoretical approach based on intrinsic ignition and the concept of transfer entropy (TE) to assess the spatiotemporal dynamics after VIM-MRgFUS. Eighteen ET patients (mean age 71.44 years) underwent repeated 3T resting-state functional magnetic resonance imaging combined with Clinical Rating Scale for Tremor (CRST) assessments one day before (T0) and one month (T1) and six months (T2) post-MRgFUS, respectively. We observed increased whole brain ignition-driven mean integration (IDMI) at T1 ($p < 0.05$), along with trend increases at T2. Further, constraining to motor network nodes, we identified significant increases in information-broadcasting (bilateral supplementary motor area (SMA) and left cerebellar lobule III) and information-receiving (right precentral gyrus) at T1. Remarkably, increased information-broadcasting in bilateral SMA was correlated with relative improvement of the CRST in the treated hand. In addition, causal TE-based effective connectivity (EC) at T1 showed an increase from right SMA to left cerebellar lobule crus II and from left cerebellar lobule III to right thalamus. In conclusion, results suggest a change in information transmission capacity in ET after MRgFUS and a shift towards a more integrated functional state with increased levels of global and directional information flow.

1. Introduction

Essential tremor (ET) is a common tremor cause, with a prevalence of 0.4–3.9% [1–3]. Patients exhibit postural tremor with frequencies of 4–12 Hz [4,5], occurring predominantly in upper limbs [6] and impairing the health-related quality of life [7]. Deep brain stimulation (DBS) of the ventral intermediate nucleus (VIM), which resembles the inferior aspect of the ventroposterolateral thalamus [8], represents a therapeutic alternative for drug-refractory ET. The VIM receives cerebellar fibres via the cerebello-thalamo-cortical tract (CTCT) [9] and projects fibres to primary motor cortex (M1) [10,11] and minorly to supplementary motor area (SMA) [11], pre-SMA and premotor cortex [12]. Magnetic resonance guided focused ultrasound (MRgFUS) has emerged as an alternative stereotactic modality for VIM-lesioning [13,14]. MRgFUS creates a focal brain lesion applying thermal ablation via ultrasound [15]. Since no ferromagnetic material is implanted, post-interventional magnetic resonance imaging (MRI) measurements are less constrained than with DBS.

ET is characterized by neurodegeneration affecting the cerebellum in

* Corresponding author. Clinical Functional Imaging Group, Department of Diagnostic and Interventional Radiology, University Hospital Bonn, Bonn, Germany.
E-mail addresses: s4juluec@uni-bonn.de (J.M. Lueckel), Henning.Boecker@ukbonn.de (H. Boecker).
[1] These authors contributed equally as first authors to this work.
[2] These authors contributed equally as last authors to this work.

https://doi.org/10.1016/j.brs.2023.05.006
Received 28 October 2022; Received in revised form 30 March 2023; Accepted 8 May 2023
Available online 23 May 2023

Abbreviations

CRST	Clinical Rating Scale for Tremor
CTCT	Cerebello-thalamo-cortical tract
EC	Effective connectivity
ET	Essential tremor
IC	Independent component
IDMI	Ignition-driven mean integration
FC	Functional connectivity
M1	Primary motor cortex
MRI	Magnetic resonance imaging
MRgFUS	Magnetic resonance guided focused ultrasound
ROI	Region of interest
RsfMRI	Resting state functional MRI
SMA	Supplementary motor area
TE	Transfer entropy
VIM	Ventralis intermedius nucleus

terms of morphometric changes and loss of Purkinje cells [16–18], as well as decrease in the number of GABAergic receptors in the dentate nucleus [19]. This results in a dysregulation of the cerebello-thalamo-cortical network in ET patients compared to healthy individuals [20–23]. More specifically, ET is driven by an oscillating network, in which inferior olive, cerebellum, thalamus, M1, SMA and premotor cortex interact dynamically [24,25]. Synchronized oscillations at tremor frequency were observed between M1, premotor cortex, thalamus, cerebellum, and brainstem [26,27], and there is also evidence for a coupling of M1 and muscle activity [23–25]. This dysregulation is also reflected by decreased functional connectivity (FC) of primary sensorimotor cortex with lobules of the contralateral cerebellum, as well as increased FC of bilateral thalami with posterior cerebellar regions and vermis [22]. Again, these alterations can be linked with clinical symptomatology: Tremor severity correlates with decreased FC among cortical and cerebellar regions [22,25,28] while FC between SMA and M1 correlates negatively with tremor score, underlining the participation of the SMA in the oscillating tremor network [29]. Meanwhile, tremor severity has been shown to correlate with increased FC between right cerebellar lobules I-IV and left thalamus [25], and between pre-SMA and thalamus [30]. In conclusion, pathological synchronized oscillations [24] and altered FC states [22] play distinctive roles in ET pathophysiology.

'Information theoretical analysis' has been widely applied in neuroscience [31,32] to measure neural responses considering information quantity [31]. It assesses changes in information exchange in a network characterized by deviations of oscillations [33], local field potentials and spike trains [31]. Resting state functional MRI (rsfMRI) provides an opportunity to assess whole-brain functional dynamics [34]. Deco and Kringelbach introduced the concept of the intrinsic ignition framework to conclude on a network's integration [35]. Intrinsic ignition allows to capture propagation of brain activity and its fluctuations [35]. Efficacy in complex networks is higher, the more dynamic the flow between segregated (specialized and autonomous areas) and integrated (elevated levels of information flow) network states is [36]. Transfer entropy (TE) quantifies information transfer [37]. High TE values are associated with more integrated network states [38]. TE measures how time series of neuronal activity in one node forecast the future time series of neuronal activity in another node [37,39,40]. Interhemispheric FC and TE are disrupted in altered brain networks [41]. Effective connectivity (EC) represents the influence of one brain region on another in terms of causal dynamics and neural coupling [42]. TE-based EC allows quantification of nonlinear interactions of information transmission between brain regions [43].

Recently, we observed structural and functional alterations along the CTCT using task-fMRI and diffusion tensor imaging (DTI) in ET patients undergoing VIM-MRgFUS [44]. In this study we extend our analysis to global information flow. We hypothesize that unilateral VIM-MRgFUS, by disrupting the dominant oscillatory network activity in the CTCT, improves the capacity of information transmission at the whole brain level and leads to a more integrated network state. Additionally, we hypothesize that decrease in tremor post-MRgFUS associates with increase in information flow at the motor network level.

2. Materials and methods

2.1. Participants

26 ET patients undergoing MRgFUS treatment at the University Hospital in Bonn got included. Inclusion criteria comprised age above 18 years and a medication-refractory diagnosis of ET [45]. Patients with head tremor, structural brain changes, history of head injuries or movement disorders other than ET were excluded. Every patient provided written informed consent before enrolment. The study was conducted according to the Declaration of Helsinki. Ethical approval was given by the ethics committee of the University Hospital Bonn (Nr. 207/06).

2.2. Clinical assessment

We examined the clinical rating scale for tremor (CRST) according to Fahn and Tolosa [46] that is widely applied as a score in clinical assessment of ET [47]. The CRST consists of three subscales (A, B and C), each rating a different dimension of the tremor severity. Subscale A quantifies tremor severity in terms of a resting, posture holding and action component for nine parts of the body, divided to left and right. Subscale B relates to the action tremor of the upper extremities in form of the ability to draw, write and pour water into a cup, also divided to left and right (handwriting only with dominant hand). The third subscale, subscale C, evaluates the by the patient subjectively perceived impact of the current tremor on daily activities (getting dressed, bringing liquids to the mouth, speaking etc.). We considered part B and isolated the subscore of upper extremity tremor rating of part A to create a modified CRST-subscale ("AB subscale") consisting of 7 items resulting in a maximum of 28 points. The score was calculated for treated and non-treated side separately.

2.3. MRgFUS intervention

Patients underwent pre-interventional head CT scanning to determine feasibility of MRgFUS according to the skull density ratio. During intervention, patients received focal MRgFUS lesioning of the ventralis intermedius nucleus (VIM) of the corresponding tremor-dominant hand (14 right-dominant tremor, 4 left-dominant tremor). Thermal ablation (ExAblate Neuro 4000, Insightec) was used to create a lesion in the VIM using ultrasound waves as described previously [44]. Before the final lesion was placed, the sonification first induced reversible test lesions. After clinical assessment of the change in the patient's tremor by a neurologist, coordinates were readjusted to the best possible outcome. MRgFUS inclusion criteria are detailed in German Clinical Trials registry (DRKS00016695).

2.4. MRI procedures

2.4.1. Acquisition

ET patients underwent MRI examinations at three time points (T0, T1 and T2) at the Clinic for Neuroradiology at the University Hospital Bonn. RsfMRI data was acquired axially with a 3T MRI-scanner and an eight channel head neck spikes arrays coils. The images were acquired as following: Voxel size: 3.59 × 3.59 × 3.59 mm^3, repetition time (TR): 2.595 s, echo time (TE): 5.5001 ms, flip angle: 90°, no gap. Each scan

produced 250 rsfMRI images in a scan duration of 10.81 min. Individuals were told to close their eyes without focusing on particular thoughts and without falling asleep. Structural data was acquired using a Magnetization Prepared-Rapid Gradient Echo (MPRAGE) 3D T1-weighted sequence with the parameters: voxel size: 1 × 1 × 1 mmm^3, matrix size 256 × 256 mm, repetition time (TR): 7.293 ms, echo time (TE): 3.93 ms, flip angle (FA): 15° and scan duration: 4:39 min.

2.4.2. Imaging data analysis

2.4.2.1. Preprocessing. Data was pre-processed using the FEAT software included in FSL toolbox (FMRIB Software Library; https://fsl.fmrib.ox.ac.uk/fsl/fslwiki/FEAT). Pre-processing included skull striping, motion correction, high pass temporal filtering (0.01 Hz) and spatial smoothing (7 mm). In addition, independent component analysis (ICA) option was turned on in order to create individual independent components (ICs). These ICs were labelled for signal and noise components in a small sample of 10 subjects. ICA-based denoising (ICA fix, manual labelling) and registration to the T1-weighted anatomical image was conducted. Data got excluded due to motion artefacts at a threshold of >0.5 mm mean framewise displacement. For analysis purposes, the data of the patients with MRgFUS of the right VIM, was flipped. Automated Anatomical Labeling version 2 [48] was registered on the average brain mask for parcellation and time course extraction, i.e., to define brain nodes for information flow analysis. Time courses were extracted from 116 brain regions of interests (ROIs), were then brought to a 116 × 116 weighted correlation matrix and got processed afterwards.

2.4.2.2. Information theoretical analysis

2.4.2.2.1. Ignition-driven mean integration (IDMI). Intrinsic ignition is a measure to quantify the level of the brain's activity propagation and integration elicited by spontaneously occurring intrinsic endogenous events in the brain regions [49]. To characterize intrinsic ignition, first the intrinsic driving events were extracted for each timepoint from all 116 brain regions. Thereafter, the network integration elicited by each of the endogenous events was calculated. Prior to event extraction, each BOLD signal was narrow band pass filtered (0.04–0.07 Hz) to evaluate the synchrony, as this frequency band captures more relevant information in terms of brain function [50]. In addition, selection of such narrow filter was based on the prominence of brain activity related to sensorimotor function in regions like thalamus [51]. The intrinsic events were defined for every brain region characterized by large fluctuations in the BOLD signal. To this end, the measured BOLD-activity was binarized at a threshold (event threshold) by applying z-scores at time t (z(t)) [35]. An event occurs at a node when the BOLD activity z (t) surpasses a threshold of $\theta = 1.5$ of standard deviation at every given brain region. The BOLD signal is considered 1 if z (t) is higher than the calculated threshold and is considered to be 0 if z (t) is lower than the calculated threshold [52] giving rise to a binarized phase locking matrix. The mean event threshold in consequence is calculated conditionally on the present level of ignition events. As soon as an event in a brain region reaches above the threshold, the effect of the triggering event on the integration in the global network is measured over a time window of $t \rightarrow t + 4$ TR (for visual display, please see Fig. 1A). The network integration was computed through a phase-based FC matrix. Instead of Pearson's correlation, FC is calculated using the phase-locking values between two BOLD signals in order to avoid errors of computing correlation over short windows [55].

For this, the instantaneous phases $\varphi_k(t)$ were computed using the Hilbert transform for each BOLD signal individually [50]. This yields the associated analytical signal which represents a narrow band signal s(t) in the time domain as a rotating vector with an instantaneous phase $\varphi(t)$ and an instantaneous amplitude, A(t). That is, $s(t) = A(t)\cos(\varphi(t))$. Given the instantaneous phases $\varphi_j(t)$ and $\varphi_k(t)$ of two brain regions, the

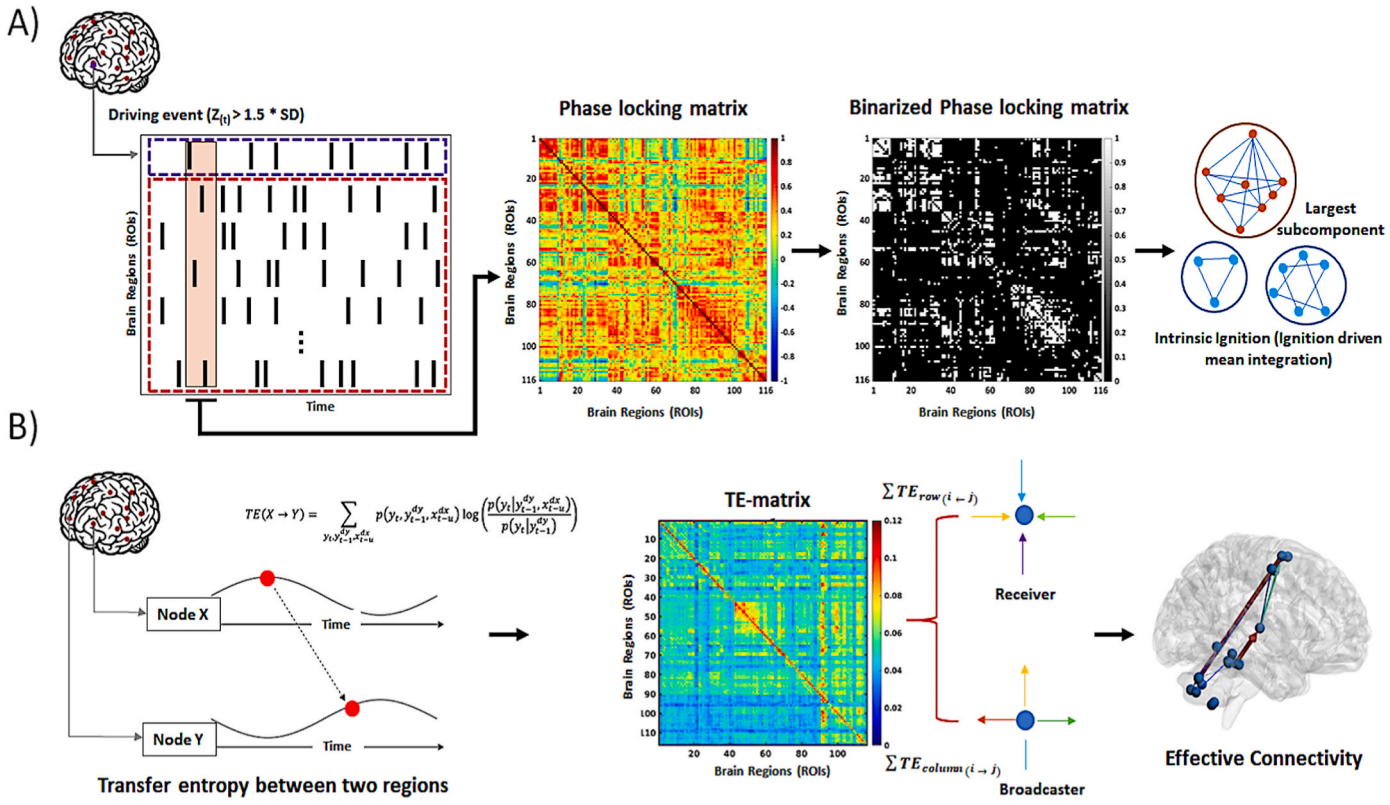

Fig. 1. Computational methods: A) shows the ignition driven mean integration calculation from time series extraction to integration value calculation; B) shows the transfer entropy analysis pipeline that leads to model free effective connectivity between the different brain regions. $Z_{(t)}$ = values of event in fisher's z; SD = standard deviation; TE = transfer entropy.

pairwise synchronization $P_{jk}(t)$ was defined as the cosine similarity of the two phases expressed as:

$$P_{jk}(t) = cos\left(\left|\varphi_j(t) - \varphi_k(t)\right|\right) \quad (1)$$

P(t) is the phase-interaction matrix at a given time t, which represents the instantaneous phase synchrony among the different brain regions (i.e., phase-based FC). Then, the integration value computed for each endogenous events, is thus calculated as area-under-the-curve for the largest subcomponent of the binarized FC matrix. These integration values of all spiking events across time are then averaged to calculate the global ignition-driven mean integration (IDMI). Ignition variability across time is able to classify brain regions in terms of functional variability, i.e., metastability. It is measured as the variability of integration in terms of alterations in the intrinsic ignition (i.e., the standard deviation of the ignition-driven integration) [35].

2.4.2.2.2. Transfer entropy framework to assess dynamic brain information exchange. To characterize how endogenous neural activity alters the brain causal-effect or information exchange after interventional lesion created in the thalamus, we adopted the Renyi's Transfer Entropy (TE) framework [53]. TE quantifies the amount of information transfer between pairs of brain regions and infers on causality of neural connections [37], based on the concept of transition probability (Fig. 1B). We have computed the transfer entropy using Renyi's TE framework [53,54]. Considering two concurrently sampled BOLD time series (in ROIs), a source ROI X = {x1, x2, x3, …, xN}, and a target ROI Y = {y1, y2, y3, …, yN}, the TE(X→Y) is then estimated as the reduced amount of uncertainty in future signals of target ROI Y by knowing the past signals of source ROI X. This can be seen as observational causality (i.e., effective connectivity) or the flow of information from X to Y, for an interaction time u. The TE(X→Y) can be computed from conditional entropies expressed as follows:

$$TE_{(X\to Y)} = \sum_{y_t, \mathbf{y}_{t-1}^{dy}, \mathbf{x}_{t-u}^{dx}} p\left(y_t, \mathbf{y}_{t-1}^{dy}, \mathbf{x}_{t-u}^{dx}\right) \log\left(\frac{p\left(y_t \middle| \mathbf{y}_{t-1}^{dy}, \mathbf{x}_{t-u}^{dx}\right)}{p\left(y_t \middle| \mathbf{y}_{t-1}^{dy}\right)}\right) \quad (2)$$

In this equation t represents the time points and u ∈ N is the interaction delay between the source ROI X and the target variable ROI Y. The *dx* and *dy* are the signal block length of X and Y respectively and p(·) is the probability mass function [53]. The above equation can be expressed as a sum of Shannon entropies as follows:

$$TE_{(X\to Y)} = H_{SE}\left(\mathbf{y}_{t-1}^{dy}, \mathbf{x}_{t-1}^{dx}\right) - H_{SE}\left(y_t \mathbf{y}_{t-1}^{dy}, \mathbf{x}_{t-1}^{dx}\right) + H_{SE}\left(y_t \mathbf{y}_{t-1}^{dy}\right) - H_{SE}\left(\mathbf{y}_{t-1}^{dy}\right) \quad (3)$$

Here H_{SE} is the Shannon entropy. Afterwards, the Shannon entropy was generalised to Renyi's α-order TE by avoiding the intermediate step of probability distribution estimation. Finally, using the kernel-based formulation of Renyi's α-order entropy for joint and marginal probability distributions, TE can be extracted from kernel matrices [53]. In this study, we considered α = 2 to be neutral to weight for the Renyi's transfer entropy [54]. The TE_{α} from X to Y expressed as:

$$TE_{2\ (X\to Y)} = H_2\left(K_{\mathbf{Y}_{t-1}^{dy}}, K_{\mathbf{X}_{t-1}^{dx}}\right) - H_2\left(K_{y_t} K_{\mathbf{Y}_{t-1}^{dy}}, K_{\mathbf{X}_{t-1}^{dx}}\right) + H_2\left(K_{y_t} K_{\mathbf{Y}_{t-1}^{dy}}\right) - H_2\left(K_{\mathbf{Y}_{t-1}^{dy}}\right) \quad (4)$$

Here H is the Shannon entropy and K is the kernel matrices, which holds element of $k_{i,j} = k(a_i,a_j)$, with $k_{ij}(\cdot,\cdot)$ is a positive definite and infinitely divisible kernel function. The matrix K_{y_t,a_i,a_j} are the value of BOLD time series Y at time *i* and *j*. Regarding the selection of parameters involved in the TE computation, the embedding delay τ was set to 1 autocorrelation time (ACT) [43]. The embedding dimension d and the interaction delay u were set in an experiment-dependent fashion, after a heuristic search intended to maximize performance [53,54]. The resultant TE matrix (NxN matrix; N=ROIs) has an asymmetric nature and represents the causal interaction between brain regions. The asymmetric nature allows us to assess the role of brain regions in accordance to whole brain dynamics as nodal broadcaster (TE-Out) and receiver (TE-In). The broadcasting capacity of a region '*i*' is calculated as the sum of all out-information flow exerted by region i on foreign brain areas, whereas the receiving or integration capacity of a region is calculated by the sum of information from the whole brain to individual node regions as follows:

$$Broadcasting\ (TE-Out) = \sum_{j=1}^{N} TE_{ij} \quad (5)$$

$$Receiving\ (TE-In) = \sum_{j=1}^{N} TE_{ji} \quad (6)$$

Conceptually, broadcasting (TE-Out) represents the influence that one region *i* exerts over the whole network and receiving (TE-In) represents how sensitive or influential a region is.

2.5. Statistical analysis

The clinical rating scale for tremor (CRST) was analysed using IBM SPSS 28 (SPSS Inc., Chicago, Illinois). To compare tremor scores in the treated and the non-treated hand at three timepoints, we created a 2 × 3 repeated measures ANOVA with the factors treatment (treatment vs. no treatment) and time (T0, T1, and T2). If sphericity was not met, a correction of degrees of freedom according to Greenhouse-Geisser was carried out.

To analyse information processing measures, we performed comparisons pre-to-post intervention at whole brain level. We then looked at the motor network implemented by Buijink et al. (2015) [25] to assure the intervention's effect on the motor network. That network included precentral gyrus; supplementary motor area (SMA); thalamus; cerebellar lobule I–IV; cerebellar lobule V; cerebellar lobule VI; and cerebellar lobule VIII, bilaterally [25]. We implemented pairwise comparisons in order to compare the groupwise and nodewise intrinsic ignition and TE T0 to T1, T0 to T2, and T1 to T2. Groupwise comparisons were corrected for multiple comparisons using Bonferroni's method and significant results were reported at $p < 0.017$ (0.05/3). Nodewise (116 nodes) comparisons of the intrinsic ignition and TE measures were corrected for the multiple comparisons using permutation-based method [55]. Results were reported at $p < 0.05$, after correcting for family-wise error. We also measured the effect sizes for comparisons and reported them respectively with the statistics.

3. Results

3.1. Participants

Of the 26 included patients, four showed increased mean framewise displacement values, three problems in image acquisition, and one treatment failure. The final sample consisted of 18 patients (14 males, 4 females; age 71.44 with a range of 32–88). 14 patients showed right-dominant, 4 left-dominant postural tremor. The side more severely affected was treated by MRgFUS of the contralateral ventralis intermedius (VIM) nucleus (VIM-lesion left/right: 14/4). The onset of tremor occurred at the age of 43.56 years on average with a range of 8–71 years (duration of tremor symptoms at the day of intervention 27.89 years on average with a range of 4–58 years). 66.67% of the patients reported positive family history of tremor and 72.22% affirmed alcohol sensitive tremor reduction. Before intervention, the patients had received an average of 2.94 (in a range of 1–6) different medications to relieve tremor. Mean skull density ratio amounted to 0.46 (in a range of 0.32–0.66). For detailed information on the clinical characteristics see Table 1.

In all patients, tremor medications were stopped 1 week prior to MRgFUS treatment. 8 patients had no preexisting tremor medication in direct advance to the intervention, 5 patients were able to stop tremor medication post-MRgFUS, 4 patients reduced their dose of tremor

Table 1
Demographic and clinical characteristics.

Measures		Median (Range)
Age (Years)		75 (32–88)
Onset (Age)		47 (8–71)
Duration (Years)		26 (4–58)
Skull Density Ratio		0.48 (0.32–0.66)
CRST (T0)	**Treated hand**	18.89 ± 4.34
Mean ± SD	**Non treated hand**	16.11 ± 5.51
CRST (T1)	**Treated hand**	4.44 ± 2.36
Mean ± SD	**Non treated hand**	15.50 ± 6.20
CRST (T2)	**Treated hand**	5.11 ± 3.79
Mean ± SD	**Non treated hand**	15.56 ± 6.70

Presentation in form of median and range for demographic data. Presentation in form of mean and standard deviation for clinical scores. CRST = Clinical Rating Scale for Tremor; T0 = pre-MRgFUS; T1 = 1-month post-MRgFUS; T2 = 6-months post-MRgFUS; SD = standard deviation.

medication and only one patient needed consistent tremor medication post-MRgFUS compared to pre-MRgFUS.

3.2. Clinical rating scale for tremor (CRST)

For the factor time (T0, T1, and T2), a significant main effect in CRST was found [$F(2, 16) = 71.69$, $p < 0.001$, $\eta_p^2 = 0.90$]. For the factor treated hand/non-treated hand, a significant main effect was found [$F(1, 17) = 31.62$, $p < 0.001$, $\eta_p^2 = 0.65$]. We also observed an interaction effect between time and treatment [$F(1.503, 16) = 98.40$, $p < 0.001$, $\eta_p^2 = 0.85$]. For the treated hand, Bonferroni corrected (0.05/9 = 0.005) post-hoc t-tests showed a significant difference between T0 and T1 ($t(17) = 16.36$, $p < 0.001$, $d = 3.86$) with a higher CRST at T0 (18.89 ± 4.34) than T1 (4.44± 2.36). The CRST in the treated hand also showed a significant difference between T0 and T2 ($t(17) = 12.25$, $p < 0.001$, $d = 2.89$) with a lower CRST at T2 (5.11± 3.79). No significant difference was found between T1 and T2 for the CRST of the treated side ($t(17) = -0.86$, $p = 0.402$, $d = -0.20$). The CRST scores at T0 were not significantly different in the treated (18.89± 4.34) compared to the non-treated hand (16.11± 5.51), ($t(17) = 2.92$, $p = 0.010$, $d = 0.69$). At T1, a significantly lower tremor score for the treated hand (4.44± 2.36) compared to the non-treated hand (M = 15.50 ± 6.20) was observed ($t(17) = -8.25$, $p < 0.001$, $d = -1.95$) with a stable effect at T2 (treated hand: 5.11± 3.79; non-treated hand: 15.56± 6.70; $t(17) = -6.98$, $p < 0.001$, $d = -1.65$). Hence, in the treated hand, at T1 a significant reduction of the CRST score by 76.73 ± 11.35% compared to T0 was found. The tremor score in the treated hand at T2 compared to the T0 remained significantly reduced by 72.99 ± 18.64%. In the non-treated hand, there was no significant change in the CRST score post-MRgFUS (T1 vs. T0: $t(17) = -0.78$, $p = 0.444$, $d = -0.18$; T2 vs. T0: $t(17) = -0.62$, $p = 0.546$, $d = -0.14$; T2 vs. T1: $t(17) = 0.07$, $p = 0.942$, $d = 0.02$). Display of the clinical results can be found in Table 1 and Fig. 2.

3.3. Information theoretical analysis

3.3.1. Ignition-driven mean integration (IDMI)

Mean event threshold significantly increased at T1 ($t(17) = 2.97$, $p = 0.009$, $d = 0.70$) but was no longer significantly elevated at T2 ($t(17) = 0.66$, $p = 0.52$, $d = 0.15$) in comparison to T0. Similarly, compared to T0, mean IDMI values showed a significant increase on a global level at T1 ($t(17) = 3.34$, $p = 0.004$, $d = 0.75$), while no significant difference was observed at T2 ($t(17) = 1.47$, $p = 0.16$, $d = 0.35$). There were no significant differences between T2 and T1 ($t(17) = 1.09$, $p = 0.29$, $d = 0.26$) in mean IDMI (Fig. 3A, left side). In Fig. 3A (right side) the nodewise course of IDMI at T0, T1 and T2 is represented. Over all nodes IDMI values rise at T1 in comparison to T0 values. In the nodewise comparisons, we found a significant ($p < 0.05$) increase in IDMI comparing T1 to T0 in brain regions including those belonging to the

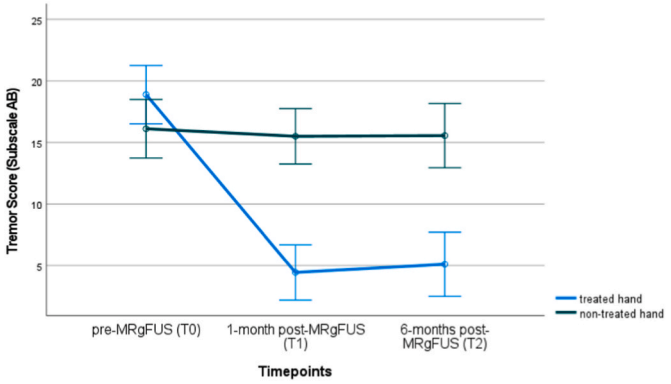

Fig. 2. Visualisation of the tremor-subscore AB of the upper extremity at pre-MRgFUS (T0), 1-month post-MRgFUS (T1) and 6-months post-MRgFUS (T2) for the treated (blue) and non-treated (green) hand. The error bars display the 95% confidence interval of the CRST average of the 18 included patients. MRgFUS: magnetic resonance guided focused ultrasound, CRST: clinical rating scale of tremor. (For interpretation of the references to colour in this figure legend, the reader is referred to the Web version of this article.)

tremor related motor network (see Table 2, Fig. 3B). At T2 IDMI values compared to T0 remained significantly increased in left ($t(17) = 3.25$, $p = 0.027$, $d = 0.77$) and right ($t(17) = 3.19$, $p = 0.031$, $d = 0.75$) olfactory cortex (Fig. 3C). Constraining the analysis to the nodes of the motor network, significant increases were observed at T1 in the right supplementary motor area (SMA) ($t(17) = 3.13$, $p = 0.046$, $d = 0.74$), left ($t(17) = 4.50$, $p = 0.005$, $d = 1.06$) and right thalamus ($t(17) = 4.58$, $p = 0.004$, $d = 1.08$), left cerebellum lobule crus II ($t(17) = 3.10$, $p = 0.049$, $d = 0.73$), right cerebellum lobule IV/V ($t(17) = 3.30$, $p = 0.036$, $d = 0.78$), right cerebellum lobule VIII ($t(17) = 3.24$, $p = 0.038$, $d = 0.76$) and vermis lobule IV/V ($t(17) = 3.34$, $p = 0.034$, $d = 0.79$) (see Fig. 3D). At T2 compared to T0, IDMI values showed no significant difference (small effect sizes) within the motor network related nodes.

3.3.2. Transfer entropy (TE-In and TE-Out)

TE-In averaged over the whole brain showed a trend ($t(17) = 2.05$, $p = 0.056$, $d = 0.48$) at T1 compared to T0. No significant changes were found in TE-In at the node level in whole brain analysis. While looking at the motor network nodes, we found a significant increase in TE-In in the right precentral gyrus ($t(17) = 4.48$, $p = 0.003$, $d = 1.06$) as well as trends in the right SMA ($t(17) = 2.85$, $p = 0.058$, $d = 0.67$) and the left cerebellum lobule crus II ($t(17) = 2.78$, $p = 0.065$, $d = 0.66$) for T1 compared to T0 (Fig. 4B).

TE-Out averaged over the whole brain also showed a trend ($t(17) = 2.05$, $p = 0.056$, $d = 0.48$) at T1 compared to T0. No significant changes were found in TE-Out at the node level in whole brain analysis. Limiting the analysis to motor network nodes reported significant ($p < 0.05$) increases in TE-Out for T1 compared to T0 in left ($t(17) = 3.11$, $p = 0.031$, $d = 0.73$) and right ($t(17) = 3.06$, $p = 0.034$, $d = 0.72$) supplementary motor area (SMA), left cerebellum lobule III ($t(17) = 3.04$, $p = 0.036$, $d = 0.71$) as well as trends in left thalamus ($t(17) = 2.82$, $p = 0.053$, $d = 0.66$) and right cerebellum lobule III ($t(17) = 2.67$, $p = 0.068$, $d = 0.63$) (Fig. 4C).

3.3.3. Transfer entropy based effective connectivity

Different patterns of effective connectivity (EC) could be identified at T0, T1 and T2 (Fig. 4A). Due to the large number of multiple comparisons, we found no significant changes in EC at the whole brain level. In the motor network we observed significantly ($p < 0.05$) increased EC at T1 from right supplementary motor area (SMA) to left cerebellum lobule crus II ($t(17) = 4.62$, $p = 0.037$, $d = 1.09$) as well as from left cerebellum lobule III to right thalamus ($t(17) = 4.56$, $p = 0.041$, $d = 1.07$) (Fig. 4D). Applying an effect size approach using Cohen's d and limiting it to larger

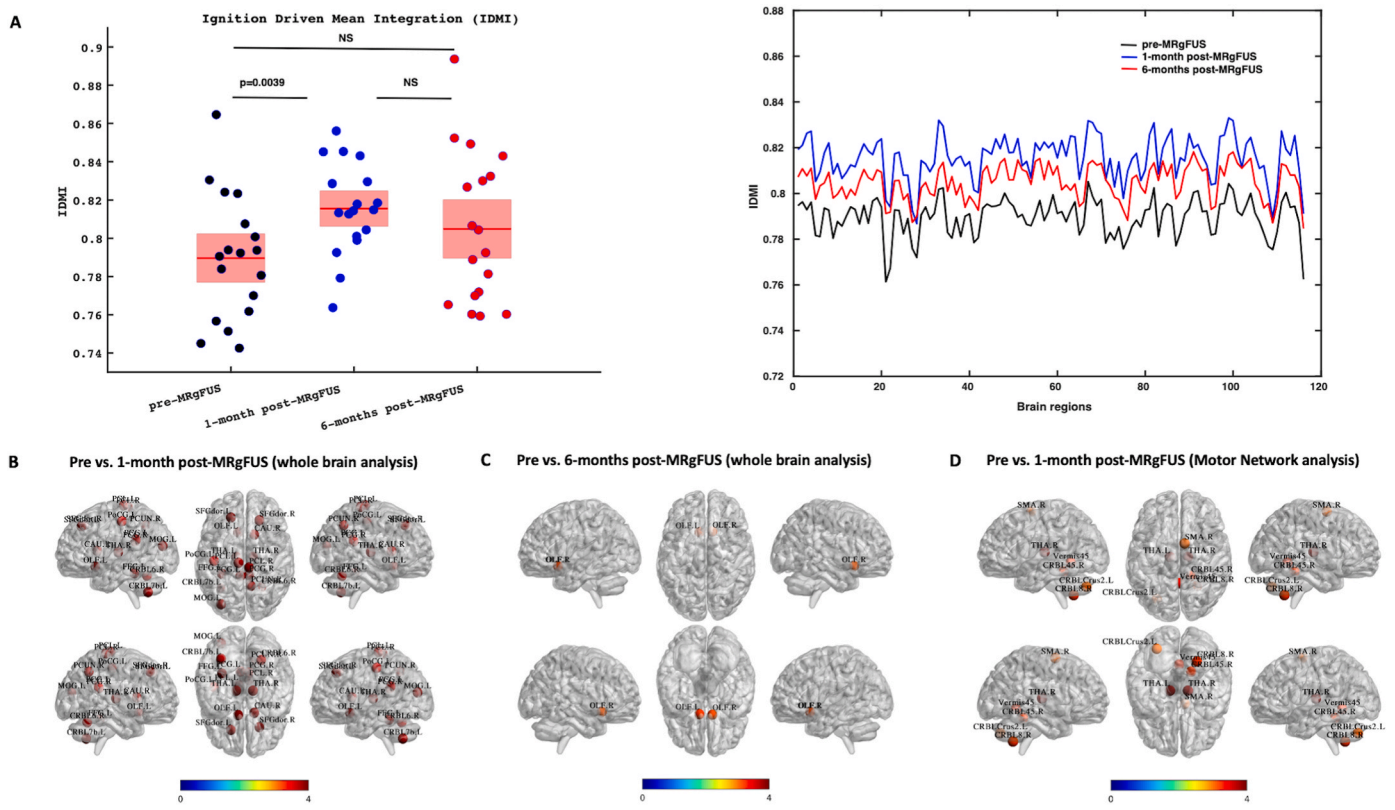

Fig. 3. Intrinsic ignition results: A) Left side: Mean of the global ignition-driven mean integration (IDMI) for the group average and IDMI according to regional distribution at all three timepoints (pre-MRgFUS (T0), 1-month post-MRgFUS (T1) and 6-months post-MRgFUS (T2)) and mean value of the global IDMI for every single subject (grey). Right side: Increase over all nodes in IDMI 1-month post-MRgFUS (blue) compared to pre-MRgFUS (black). IDMI values decrease over all 116 nodes 6-months post-MRgFUS (red) compared to 1-month post-MRgFUS but do not revert to pre-interventional state; B) Significant increase ($p < 0.05$) in IDMI 1-month post-MRgFUS compared to pre-MRgFUS considering all global nodes. C): Significant increase ($p < 0.05$) in IDMI 6-months post-MRgFUS compared to pre-MRgFUS considering all global nodes. D) Significant increase ($p < 0.05$) in IDMI 1-month post-MRgFUS considering only nodes that participate in the motor network. 6-months post-MRgFUS no nodes remain significantly increased compared to the pre-MRgFUS state when only considering nodes that are part of the motor network which is why display of this comparison is not included. MRgFUS: magnetic resonance guided focused ultrasound, and L: left, R: right hemispheres. (For interpretation of the references to colour in this figure legend, the reader is referred to the Web version of this article.)

Table 2
Nodewise IDMI changes at 1-month post compared to Pre-MRgFUS in whole-brain analysis.

AAL regions	Anatomical Region	Side	MNI coordinates (mm)			t-value	p-value	Effect size
			X	Y	Z			Cohen's d
3	Dorsal superior frontal gyrus	Left	−18.45	34.81	42.20	4.96	0.006	1.17
4	Dorsal superior frontal gyrus	Right	21.90	31.12	43.82	3.97	0.030	0.93
21	Olfactory Cortex	Left	−8.06	15.05	−11.46	4.10	0.025	0.97
35	Posterior cingulate gyrus	Left	−4.85	−42.92	24.67	3.80	0.038	0.89
36	Posterior cingulate gyrus	Right	7.44	−41.81	21.87	3.72	0.043	0.87
51	Middle occipital gyrus	Left	−32.39	−80.73	16.11	3.92	0.033	0.92
55	Fusiform gyrus	Left	−31.16	−40.03	−20.23	3.99	0.029	0.94
57	Postcentral gyrus	Left	−42.46	−22.63	48.92	3.61	0.049	0.85
68	Precuneous	Right	9.98	−56.05	43.77	3.85	0.035	0.91
69	Paracentral Lobule	Left	−7.63	−25.36	70.07	3.86	0.035	0.91
70	Paracentral Lobule	Right	7.48	−31.59	68.09	3.91	0.033	0.92
72	Caudate	Right	14.84	12.07	8.09	3.91	0.033	0.92
77	Thalamus	Left	−10.85	−17.56	7.98	4.50	0.013	1.06
78	Thalamus	Right	13.00	−18.00	8.09	4.58	0.012	1.08
100	Cerebellum lobule VI	Right	24.69	−58.32	−23.65	3.90	0.033	0.92
101	Cerebellum lobule VII	Left	−32.36	−59.82	−45.45	3.81	0.037	0.90

Nodes that show significant ($p < 0.05$) increases in IDMI when considering all nodes at whole brain level. Left: left hemisphere, Right: right hemisphere, AAL: Automated Anatomical Labeling, MNI: Montreal Neurological Institute.

effects ($d > 0.80$) showed an additional increase in Transfer Entropy (TE) based EC from left thalamus to left precentral gyrus ($d = 0.86$), as well as among other motor network areas at T1 (Supplementary Table 1; Supplementary Fig. 1). We did not observe significant changes in EC at T2 compared to T0 in the motor network. Applying an effect size approach using Cohen's d we observed a medium effect size for the EC in the motor network for the comparison between T2 and T0 (Supplementary Table 2; Supplementary Fig. 2).

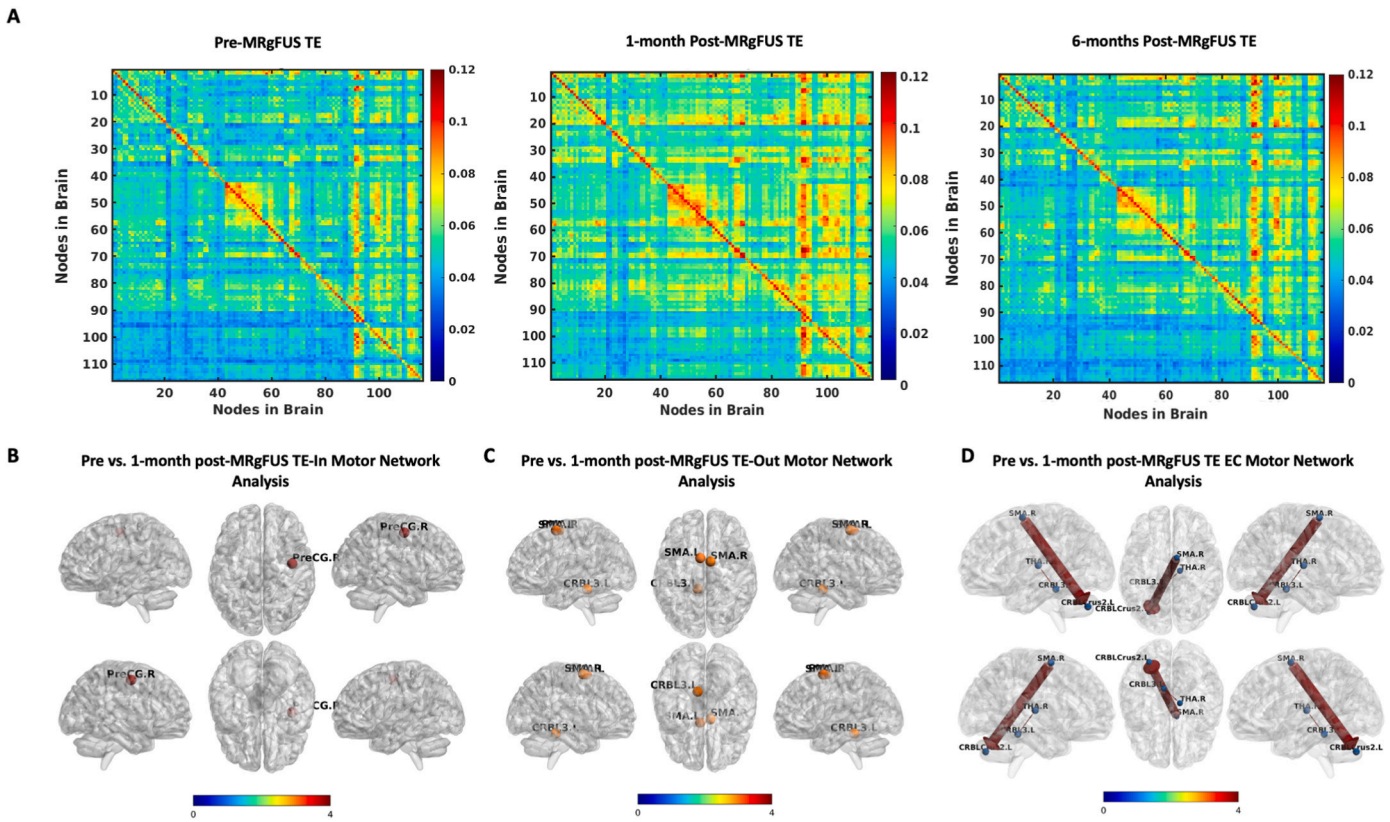

Fig. 4. Transfer entropy (TE) changes at pre, 1-month post and 6-months post-MRgFUS. A) TE matrix at pre, 1-month post and 6-months post combining TE-In and TE-Out at each node, B) Increased TE-In in the motor network at 1-month post-MRgFUS, C) Increased TE-Out in the motor network at 1-month post-MRgFUS and D) Increased effective connectivity in motor network at 1-month post-MRgFUS and arrows show the direction of change. Bar plot in Figure B), C) and D) represents t-values at $p < 0.05$, corrected for multiple comparisons based on the permutation method. CRBL: cerebellum, SMA: supplementary motor area, THA: thalamus, PreCG: precentral gyrus, and L: left, R: right hemispheres, respectively.

3.3.4. *Clinico-radiological correlations*

The relative reduction in the clinical rating scale (CRST) subscore AB for the treated arm showed a correlation with relative increase in regional Transfer Entropy Out (TE-Out) T1 vs. T0: A negative correlation between the extent of reduction in the CRST in the treated arm and TE-Out values in the left ($r = -0.52$, $p = 0.026$) and the right ($r = -0.53$, $p = 0.023$) SMA. Additionally, increase in TE-In at the right precentral gyrus showed a trend in negative correlation ($r = -0.43$, $p = 0.074$) with relative CRST reduction in the treated arm (Fig. 5).

4. Discussion

To the best of our knowledge, this study is the first using an information theoretical approach to unravel whole-brain and regional network changes in ET patients after MRgFUS of the ventralis intermedius (VIM) nucleus. Our study revealed increases in ignition-driven mean integration (IDMI), Transfer Entropy (TE), and effective connectivity (EC) indicating higher levels of global information flow post-MRgFUS. Increased IDMI was significant at global and motor network levels. Additionally, the relative reduction in tremor scores in the treated arm 1-month post-MRgFUS correlated significantly with increased values of TE-Out (left and right supplementary motor area

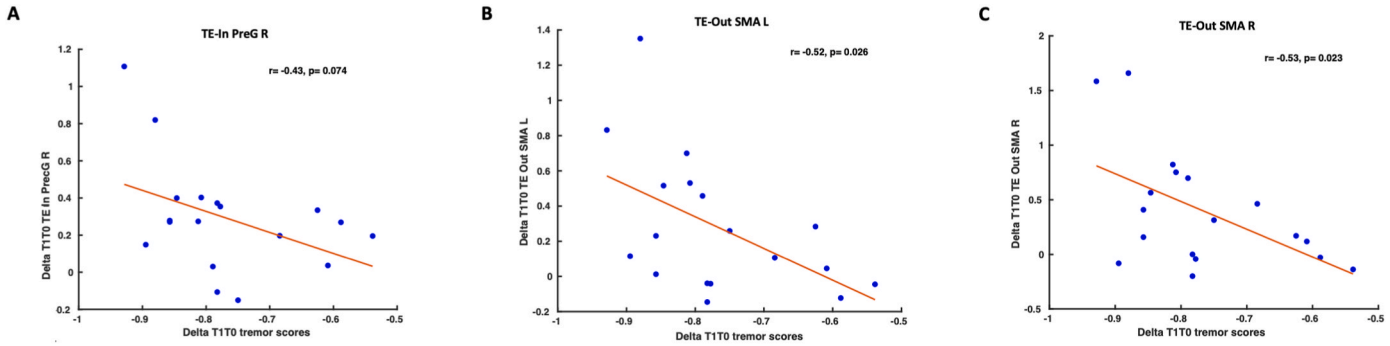

Fig. 5. Clinico-radiological correlations found between relative reduction in tremor scores in the treated arm and relative change in transfer entropy (TE) 1-month post-MRgFUS (T1) vs. pre-MRgFUS (T0). A) Correlation of relative reduction in tremor score in the treated arm with relative change in TE-In in PrecG R, B) Correlation of relative reduction in tremor score in the treated arm with relative change in TE-Out in SMA L and, C) Correlation of relative reduction in tremor score in the treated arm with relative change in TE-Out in SMA R. PrecG: precentral gyrus, SMA: supplementary motor area; L: left; R: right.

(SMA)) and at trend levels with TE-In (right precentral gyrus), indicating clinical relevance. The observed increases in information transfer capacity post-MRgFUS tended to remain at 6-month with effect sizes in the small-to-medium range. In addition, TE-based EC showed an increase in interhemispheric connectivity within the tremor network, which was most pronounced at T1, but still evident at T2.

The ability to propagate anterograde and retrograde information [35] is a prerequisite for efficient brain function in highly complex networks [56,57]. Our findings can thus be interpreted as follows: The significant increase in global IDMI 1-month post-MRgFUS refers to an elevated level of the nodes' capability to propagate neuronal activity, resulting in a shift to an integrated whole-brain network state. Given the fact that ET pathophysiology is characterised by a decrease in functional connectivity (FC) among tremor generating areas and altered functional integrity [25,58], we conclude on a shift towards a more physiological network state post-MRgFUS. In line with these observations, an earlier study using standard FC analyses also indicated whole-brain network reconfigurations post-MRgFUS of the VIM [58]. Importantly, a recent study in ET patients by Bhardwaj et al. showed decreased intrinsic ignition in ET patients compared to healthy controls that normalized to control levels after a single session of neuromodulation using repetitive transcranial magnetic stimulation in ET [59]. Secondly, analysis of the local motor network nodes unravelled significant increases in IDMI in bilateral thalami, in SMA and in both cerebellar hemispheres 1-month post-MRgFUS (small effect sizes at 6-month post-MRgFUS). Findings thus highlight changes in dynamic brain activity in areas known to constitute the tremor generating network of ET [24]. This network has frequently been demonstrated to consist of the cerebello-thalamo-cortical tract (CTCT) [27], with the VIM projecting fibres mainly to the primary motor cortex [8,10]. Beyond this connection, studies in ET patients have established relevant connections to SMA [60,61]. Considering the presumed pathophysiology, the significant increase in local IDMI as a measure of integration in the CTCT, indicates disruption of unidirectional pathological neuronal firing pre-MRgFUS and a higher level of global integration post-MRgFUS. These effects were pronounced at 1-month and decreased at 6-months post-MRgFUS.

Information-broadcasting appears significantly increased 1-month post-MRgFUS in the SMA of both hemispheres as well as in left cerebellar lobule III, suggesting elevated levels of information transfer out of these nodes post-MRgFUS. With reference to the pathological oscillating network theory and the particular role of the CTCT [25,62], we speculate that the significant increases in TE-Out in SMA and cerebellum indicate enhanced information transfer in the local tremor network post-MRgFUS, approaching a more physiological network state due to a reduction of superimposing pathological rhythmic oscillations. Also, our findings go along with previous research stating a lower amplitude of low-frequency fluctuation of the blood oxygen level dependent (BOLD) signal in the SMA and less effective connectivity between each SMA and the ipsilateral primary motor hand area in ET patients compared to healthy controls [29]. These findings correlate with tremor severity [29]. Moreover, tremor severity has been reported to positively correlate with selective connectivity between the thalamus and among other structures (putamen, parietal cortex) the pre-SMA, and between the pre-SMA and the putamen [30]. Based on the abovementioned points, increased information-broadcasting in bilateral SMA correlating with relative reduction in tremor score in the treated arm fits well with the aforementioned literature where SMA is described as a major component of the tremor network.

Another important finding is the increase in TE-In in the non-targeted precentral gyrus related with the reduction in tremor score in the treated hand. Patients suffering from ET show reduced FC from left to right precentral gyrus [63]. The effects of MRgFUS lead to increasing information input to the precentral gyrus of the non-treated hand. In line to this, a recent study found increased FC from precentral gyrus of the treated side to the precentral gyrus of the non-treated side following VIM-MRgFUS in patients with Parkinson disease [64]. Thus, we speculate that a unilateral VIM lesion disrupts the pathological unidirectional neuronal information propagation present in the ET tremor network, in turn resulting in increased functional exchange with other hemispheric regions.

We observed at 1-month post-MRgFUS EC changes along the non-targeted CTCT, that might indicate a reconfiguration of directed information flow in the other hemisphere. At the same time, we observed an increase in EC from left thalamus to left precentral gyrus that is most likely due to a reorganization of the network towards physiological information broadcasting despite the loss of structural connections. This might be based on a significant reduction in pathological oscillatory activity passing through respective pathways, which in turn leads to an increase in physiological information flow. In addition, EC changes at 6-month post-MRgFUS were recognizable in both hemispheres at medium effect sizes and may reflect a long-term reorganization of neuronal coupling with elevated levels of interhemispheric connectivity. We have to point out that the current EC data are derived from rsfMRI where no tremor activity is detected. Therefore, the role of these EC changes are difficult to relate to clinical tremor characteristics, as has been reported previously using task-fMRI [25]. Future studies are thus awaited to further examine these network reconfigurations in the targeted and non-targeted hemisphere.

Limitations are as follows: The biological basis for information theoretical changes is not entirely solved. Future studies including structural information are needed to confirm our findings. Also, our cohort is rather small and future research should include larger samples. Inclusion of healthy individuals and/or sham MRgFUS may be considered for comparative purposes and may further improve studies on the effects of VIM lesions on information flow. Although the dosage of tremor medication was fully stopped or reduced in most cases, we have to acknowledge that 28% of the patients still received tremor medication during the cause of the study. Since tremor medications were stopped 1 week prior to MRgFUS treatment, and thus at pre-treatment MRI, we cannot entirely rule out an effect of this partial and residual treatment on the follow-up MRI measurements. Given the strong clinical effects and the related specificity of our findings in dedicated CTCT circuits, we consider these effects not as major determinants of the described findings. We have to admit, however, that future longitudinal studies should consistently stop tremor medications prior to each post-interventional MRI examination.

Concluding, by applying an information theoretical approach, the current ET study reports global and motor network specific changes in information processing and flow after unilateral VIM lesioning. Post-MRgFUS, the whole-brain network shifted to higher levels of information processing, indicating a higher integrated functional network state. Functional network adaptations were observed at 6-months post-MRgFUS, however, at small-to-medium effect sizes. The results indicate an increase in information transfer capacity with elevated levels of information flow after VIM-MRgFUS. Beyond these global network adaptations, local increases in information-broadcasting were correlated with tremor score reductions in the treated arm, highlighting the measurements' clinical relevance.

Funding

The MRgFUS system was funded by the German Research Foundation (INST 1172/64-1) and the University of Bonn's Faculty of Medicine.

This study was funded by the 'SciMed-Promotionsstipendium' as part of the BONFOR research funding program of the medical faculty at University Bonn.

Credit author statement

Julia Lueckel: Lead, Data Analysis, Writing – original draft, Writing – review & editing, review and editing; **Neeraj Upadhyay**: Co-Lead, Investigation, Formal analysis, Writing – Methodology, Methods and

Results, Writing – review & editing, review and editing; **Veronika Purrer**: Data acquisition, MRgFUS treatment, and clinical assessments, Writing – review & editing; **Angelika Maurer**: Writing – review & editing; **Valeri Borger**: MRgFUS treatment; **Alexander Radbruch**: Resource allocation for data acquisition; **Ulrike Attenberger**: Resource allocation for data analysis; **Ulrich Wüllner**: Conceptualization, Funding acquisition, Supervision, MRgFUS treatment supervision; **Rajanikant Panda**: computational method implementation, Formal analysis, Writing – review & editing, Writing – Methods, review and editing; **Henning Boecker**: Conceptualization, Formal interpretation, Funding acquisition, Supervision, Writing – review & editing, Writing - discussion, review and editing.

Declaration of competing interest

The authors declare that they have no known competing financial interests or personal relationships that could have appeared to influence the work reported in this paper.

Appendix A. Supplementary data

Supplementary data to this article can be found online at https://doi.org/10.1016/j.brs.2023.05.006.

References

[1] Louis ED, Ottman R, Hauser WA. How common is the most common adult movement disorder? estimates of the prevalence of essential tremor throughout the world. Mov Disord 1998;13(1):5–10. https://doi.org/10.1002/mds.870130105.

[2] Benito-León J. How common is essential tremor? Neuroepidemiology 2009;32(3):215–6. https://doi.org/10.1159/000195692.

[3] Malkki H. Movement disorders: novel genetic risk variants for essential tremor. Nat Rev Neurol 2016;12(12):679. https://doi.org/10.1038/nrneurol.2016.176.

[4] Benito-León J, Louis ED. Clinical update: diagnosis and treatment of essential tremor. Lancet 2007;369(9568):1152–4. https://doi.org/10.1016/S0140-6736(07)60544-3.

[5] Louis ED. The primary type of tremor in essential tremor is kinetic rather than postural: cross-sectional observation of tremor phenomenology in 369 cases. Eur J Neurol 2013;20(4):725–7. https://doi.org/10.1111/j.1468-1331.2012.03855.x.

[6] Louis ED. Clinical practice. Essential tremor. N Engl J Med 2001;345(12):887–91. https://doi.org/10.1056/NEJMcp010928.

[7] Louis ED, Machado DG. Tremor-related quality of life: a comparison of essential tremor vs. Parkinson's disease patients. Parkinsonism Relat Disorders 2015;21(7):729–35. https://doi.org/10.1016/j.parkreldis.2015.04.019.

[8] Hirai T, Jones EG. A new parcellation of the human thalamus on the basis of histochemical staining. Brain Res Rev 1989;14(1):1–34. https://doi.org/10.1016/0165-0173(89)90007-6.

[9] Gallay MN, Jeanmonod D, Liu J, Morel A. Human pallidothalamic and cerebellothalamic tracts: anatomical basis for functional stereotactic neurosurgery. Brain Struct Funct 2008;212(6):443–63. https://doi.org/10.1007/s00429-007-0170-0.

[10] Jones EG. The thalamus. Cambridge: Cambridge University Press; 2007.

[11] Klein JC, Barbe MT, Seifried C, Baudrexel S, Runge M, Maarouf M, et al. The tremor network targeted by successful VIM deep brain stimulation in humans. Neurology 2012;78(11):787–95. https://doi.org/10.1212/WNL.0b013e318249f702.

[12] Sakai ST. Cerebellar thalamic and thalamocortical projections. In: Manto M, Schmahmann JD, Rossi F, Gruol DL, Koibuchi N, editors. Handbook of the cerebellum and cerebellar disorders. Dordrecht: Springer; 2013. p. 529–47.

[13] Schuurman PR, Bosch DA, Bossuyt PM, Bonsel GJ, van Someren EJ, Bie RM de, et al. A comparison of continuous thalamic stimulation and thalamotomy for suppression of severe tremor. N Engl J Med 2000;342(7):461–8. https://doi.org/10.1056/NEJM200002173420703.

[14] Zesiewicz TA, Elble R, Louis ED, Hauser RA, Sullivan KL, Dewey RB, et al. Practice parameter: therapies for essential tremor: report of the quality standards subcommittee of the American academy of neurology. Neurology 2005;64(12):2008–20. https://doi.org/10.1212/01.WNL.0000163769.28552.CD.

[15] Haar G ter, Coussios C. High intensity focused ultrasound: physical principles and devices. Int J Hyperther 2007;23(2):89–104. https://doi.org/10.1080/02656730601186138.

[16] Louis ED, Lee M, Babij R, Ma K, Cortés E, Vonsattel J-PG, et al. Reduced Purkinje cell dendritic arborization and loss of dendritic spines in essential tremor. Brain 2014;137(Pt 12):3142–8. https://doi.org/10.1093/brain/awu314.

[17] Babij R, Lee M, Cortés E, Vonsattel J-PG, Faust PL, Louis ED. Purkinje cell axonal anatomy: quantifying morphometric changes in essential tremor versus control brains. Brain 2013;136(Pt 10):3051–61. https://doi.org/10.1093/brain/awt238.

[18] Lin C-Y, Louis ED, Faust PL, Koeppen AH, Vonsattel J-PG, Kuo S-H. Abnormal climbing fibre-Purkinje cell synaptic connections in the essential tremor cerebellum. Brain 2014;137(Pt 12):3149–59. https://doi.org/10.1093/brain/awu281.

[19] Paris-Robidas S, Brochu E, Sintes M, Emond V, Bousquet M, Vandal M, et al. Defective dentate nucleus GABA receptors in essential tremor. Brain 2012;135(Pt 1):105–16. https://doi.org/10.1093/brain/awr301.

[20] Benito-León J, Louis ED. Essential tremor: emerging views of a common disorder. Nat Clin Pract Neurol 2006;2(12):666–78. https://doi.org/10.1038/ncpneuro0347. quiz 2pp. following 691.

[21] Benito-León J. Essential tremor: a neurodegenerative disease? Tremor Other Hyperkinet Mov (N Y) 2014;4:252. https://doi.org/10.7916/D8765CG0.

[22] Lenka A, Bhalsing KS, Panda R, Jhunjhunwala K, Naduthota RM, Saini J, et al. Role of altered cerebello-thalamo-cortical network in the neurobiology of essential tremor. Neuroradiology 2017;59(2):157–68. https://doi.org/10.1007/s00234-016-1771-1.

[23] Yang J, Du Lei, Peng J, Suo X, Pinaya WHL, Li W, et al. Disrupted brain gray matter networks in drug-naïve participants with essential tremor. Neuroradiology 2021;63(9):1501–10. https://doi.org/10.1007/s00234-021-02653-7.

[24] Raethjen J, Deuschl G. The oscillating central network of Essential tremor. Clin Neurophysiol 2012;123(1):61–4. https://doi.org/10.1016/j.clinph.2011.09.024.

[25] Buijink AWG, van der Stouwe AMM, Broersma M, Sharifi S, Groot PFC, Speelman JD, et al. Motor network disruption in essential tremor: a functional and effective connectivity study. Brain 2015;138(Pt 10):2934–47. https://doi.org/10.1093/brain/awv225.

[26] Schnitzler A, Münks C, Butz M, Timmermann L, Gross J. Synchronized brain network associated with essential tremor as revealed by magnetoencephalography. Mov Disord 2009;24(11):1629–35. https://doi.org/10.1002/mds.22633.

[27] Schnitzler A, Gross J. Normal and pathological oscillatory communication in the brain. Nat Rev Neurosci 2005;6(4):285–96. https://doi.org/10.1038/nrn1650.

[28] Fang W, Chen H, Wang H, Zhang H, Puneet M, Liu M, et al. Essential tremor is associated with disruption of functional connectivity in the ventral intermediate Nucleus–Motor Cortex–Cerebellum circuit. Hum Brain Mapp 2016;37(1):165–78. https://doi.org/10.1002/hbm.23024.

[29] Gallea C, Popa T, García-Lorenzo D, Valabregue R, Legrand A-P, Marais L, et al. Intrinsic signature of essential tremor in the cerebello-frontal network. Brain 2015;138(Pt 10):2920–33. https://doi.org/10.1093/brain/awv171.

[30] Mueller K, Jech R, Hoskovcová M, Ulmanová O, Urgošík D, Vymazal J, et al. General and selective brain connectivity alterations in essential tremor: a resting state fMRI study. Neuroimage Clin 2017;16:468–76. https://doi.org/10.1016/j.nicl.2017.06.004.

[31] Quian Quiroga R, Panzeri S. Extracting information from neuronal populations: information theory and decoding approaches. Nat Rev Neurosci 2009;10(3):173–85. https://doi.org/10.1038/nrn2578.

[32] Dimitrov AG, Lazar AA, Victor JD. Information theory in neuroscience. J Comput Neurosci 2011;30(1):1–5. https://doi.org/10.1007/s10827-011-0314-3.

[33] Waltermann C, Klipp E. Information theory based approaches to cellular signaling. Biochim Biophys Acta 2011;1810(10):924–32. https://doi.org/10.1016/j.bbagen.2011.07.009.

[34] Deco G, Kringelbach ML. Great expectations: using whole-brain computational connectomics for understanding neuropsychiatric disorders. Neuron 2014;84(5):892–905. https://doi.org/10.1016/j.neuron.2014.08.034.

[35] Deco G, Kringelbach ML. Hierarchy of information processing in the brain: a novel 'intrinsic ignition' framework. Neuron 2017;94(5):961–8. https://doi.org/10.1016/j.neuron.2017.03.028.

[36] Tognoli E, Kelso JAS. The metastable brain. Neuron 2014;81(1):35–48. https://doi.org/10.1016/j.neuron.2013.12.022.

[37] Schreiber. Measuring information transfer. Phys Rev Lett 2000;85(2):461–4. https://doi.org/10.1103/PhysRevLett.85.461.

[38] Rommel V. Ceguerra, Joseph T. Lizier, Albert Y. Zomaya. Information storage and transfer in the synchronization process in locally-connected networks.

[39] Li M, Han Y, Aburn MJ, Breakspear M, Poldrack RA, Shine JM, et al. Transitions in information processing dynamics at the whole-brain network level are driven by alterations in neural gain. PLoS Comput Biol 2019;15(10):e1006957. https://doi.org/10.1371/journal.pcbi.1006957.

[40] Spinney RE, Lizier JT. Characterizing information-theoretic storage and transfer in continuous time processes. Phys Rev E 2018;98(1–1):12314. https://doi.org/10.1103/PhysRevE.98.012314.

[41] Mäki-Marttunen V, Diez I, Cortes JM, Chialvo DR, Villarreal M. Disruption of transfer entropy and inter-hemispheric brain functional connectivity in patients with disorder of consciousness. Front Neuroinf 2013;7:24. https://doi.org/10.3389/fninf.2013.00024.

[42] Friston KJ. Functional and effective connectivity: a review. Brain Connect 2011;1(1):13–36. https://doi.org/10.1089/brain.2011.0008.

[43] Vicente R, Wibral M, Lindner M, Pipa G. Transfer entropy–a model-free measure of effective connectivity for the neurosciences. J Comput Neurosci 2011;30(1):45–67. https://doi.org/10.1007/s10827-010-0262-3.

[44] Pohl EDR, Upadhyay N, Kobeleva X, Purrer V, Maurer A, Keil VC, et al. Coherent structural and functional network changes after thalamic lesions in essential tremor. Mov Disord 2022. https://doi.org/10.1002/mds.29130.

[45] Bhatia KP, Bain P, Bajaj N, Elble RJ, Hallett M, Louis ED, et al. Consensus statement on the classification of tremors. From the task force on tremor of the international Parkinson and movement disorder society. Mov Disord 2018;33(1):75–87. https://doi.org/10.1002/mds.27121.

[46] Fahn S, Tolosa E, Marin C. Clinical Rating Scale for Tremor 1988;2:271–80.

[47] Elble R, Bain P, Forjaz MJ, Haubenberger D, Testa C, Goetz CG, et al. Task force report: scales for screening and evaluating tremor: critique and recommendations. Mov Disord 2013;28(13):1793–800. https://doi.org/10.1002/mds.25648.

[48] Rolls ET, Joliot M, Tzourio-Mazoyer N. Implementation of a new parcellation of the orbitofrontal cortex in the automated anatomical labeling atlas. Neuroimage 2015; 122:1–5. https://doi.org/10.1016/j.neuroimage.2015.07.075.
[49] Deco G, Tagliazucchi E, Laufs H, Sanjuán A, Kringelbach ML. Novel intrinsic ignition method measuring local-global integration characterizes Wakefulness and deep sleep. eNeuro 2017;4(5). https://doi.org/10.1523/ENEURO.0106-17.2017. ENEURO.0106-17.2017.
[50] Glerean E, Salmi J, Lahnakoski JM, Jääskeläinen IP, Sams M. Functional magnetic resonance imaging phase synchronization as a measure of dynamic functional connectivity. Brain Connect 2012;2(2):91–101. https://doi.org/10.1089/brain.2011.0068.
[51] Martino M, Magioncalda P, Huang Z, Conio B, Piaggio N, Duncan NW, et al. Contrasting variability patterns in the default mode and sensorimotor networks balance in bipolar depression and mania. Proc Natl Acad Sci U S A 2016;113(17): 4824–9. https://doi.org/10.1073/pnas.1517558113.
[52] Tagliazucchi E, Balenzuela P, Fraiman D, Chialvo DR. Criticality in large-scale brain FMRI dynamics unveiled by a novel point process analysis. Front Physiol 2012;3:15. https://doi.org/10.3389/fphys.2012.00015.
[53] La Pava Panche I de, Alvarez-Meza AM, Orozco-Gutierrez A. A data-driven measure of effective connectivity based on Renyi's α-entropy. Front Neurosci 2019;13:1277. https://doi.org/10.3389/fnins.2019.01277.
[54] Wu Z, Chen X, Gao M, Hong M, He Z, Hong H, et al. Effective connectivity extracted from resting-state fMRI images using transfer entropy. IRBM 2021;42(6): 457–65. https://doi.org/10.1016/j.irbm.2021.02.007.
[55] Blair RC, Karniski W. An alternative method for significance testing of waveform difference potentials. Psychophysiology 1993;30(5):518–24. https://doi.org/10.1111/j.1469-8986.1993.tb02075.x.
[56] Sporns O, Zwi JD. The small world of the cerebral cortex. NI, vol. 2; 2004. p. 145–62. https://doi.org/10.1385/NI:2:2:145. 2.
[57] Watts DJ, Strogatz SH. Collective dynamics of 'small-world' networks. Nature 1998;393(6684):440–2. https://doi.org/10.1038/30918.
[58] Jang C, Park H-J, Chang WS, Pae C, Chang JW. Immediate and longitudinal alterations of functional networks after thalamotomy in essential tremor. Front Neurol 2016;7:184. https://doi.org/10.3389/fneur.2016.00184.
[59] Bhardwaj S, Panda R, Bharath RD, Stezin A, Khokhar SK, Prasad S, et al. Single session of rTMS enhances brain metastability and intrinsic ignition. 2022.
[60] Revuelta G, McGill C, Jensen JH, Bonilha L. Characterizing thalamo-cortical structural connectivity in essential tremor with diffusional Kurtosis imaging tractography, vol. 9. Tremor Other Hyperkinet Mov (N Y); 2019. https://doi.org/10.7916/tohm.v0.690.
[61] Akram H, Dayal V, Mahlknecht P, Georgiev D, Hyam J, Foltynie T, et al. Connectivity derived thalamic segmentation in deep brain stimulation for tremor. Neuroimage Clin 2018;18:130–42. https://doi.org/10.1016/j.nicl.2018.01.008.
[62] Dum RP. Frontal lobe inputs to the digit representations of the motor areas on the lateral surface of the hemisphere. J Neurosci 2005;25(6):1375–86. https://doi.org/10.1523/JNEUROSCI.3902-04.2005.
[63] Nicoletti V, Cecchi P, Pesaresi I, Frosini D, Cosottini M, Ceravolo R. Cerebello-thalamo-cortical network is intrinsically altered in essential tremor: evidence from a resting state functional MRI study. Sci Rep 2020;10(1):16661. https://doi.org/10.1038/s41598-020-73714-9.
[64] Stanziano M, Golfrè Andreasi N, Messina G, Rinaldo S, Palermo S, Verri M, et al. Resting state functional connectivity signatures of MRgFUS vim thalamotomy in Parkinson's disease: a preliminary study. Front Neurol 2021;12:786734. https://doi.org/10.3389/fneur.2021.786734.